Soft Matter

PAPER

View Article Online
View Journal | View Issue



Cite this: *Soft Matter*, 2018, **14**, 6102

# Conformational change and suppression of the $\Theta$-temperature for solutions of polymer-grafted nanoparticles†

Katrina Irene S. Mongcopa, ‡[a] Ryan Poling-Skutvik, ‡[b] Rana Ashkar, §[cd] Paul Butler[c] and Ramanan Krishnamoorti *[b]

Received 6th May 2018,
Accepted 30th June 2018

DOI: 10.1039/c8sm00929e

rsc.li/soft-matter-journal

We determine the conformational change of polystyrene chains grafted to silica nanoparticles dispersed in deuterated cyclohexane using small-angle neutron scattering. The cyclohexane/polystyrene system exhibits an upper-critical solution temperature below which the system phase separates. By grafting the polystyrene chains to a nano-sized spherical silica particle, we observe a significant suppression in the $\Theta$-temperature, decreasing from $\approx$38 °C for free polystyrene chains in $d_{12}$-cyclohexane to $\approx$34 °C for the polystyrene-grafted nanoparticles. Above this temperature, the grafted chains are swollen and extended from the particle surface, resulting in well-dispersed grafted nanoparticles. Below this temperature, the grafted chains fully expel the solvent and collapse on the particle surface, destabilizing the nanoparticle suspension and leading to aggregation. We attribute the suppression of the $\Theta$-temperature to a competition between entropic and enthalpic energies arising from the structure of the polymer-grafted nanoparticle in which the enthalpic terms appear to dominate.



## 1 Introduction

The phase behavior of polymer solutions and blends depends strongly on the balance of entropic and enthalpic forces, with the excess free energy of mixing captured in the classic Flory–Huggins theory[1,2] as an interaction parameter $\chi$. In dilute solutions, the thermal dependence manifests as changes in solvent quality. Depending on the value of $\chi$ and reconciled using the Flory–Krigbaum theory,[3,4] the chain conformations change dramatically in good and poor solvents.[5] In a good solvent ($\chi < 0.5$), the favorable enthalpic interactions between monomer and solvent result in a self-avoiding random walk configuration with a radius of gyration $R_g$ that scales with the degree of polymerization $N$ as $R_g \sim N^{\nu}$ with $\nu = 0.588$. Such an extended conformation reduces the configurational entropy of the chain, but this loss of entropy is offset by an increase in favorable monomer–solvent contacts. In the poor solvent limit ($\chi > 0.5$), monomer–monomer interactions become more favorable than the monomer–solvent interactions, causing chains to collapse into globules with $\nu = 1/3$. The globule state has very low configurational entropy but minimizes the unfavorable enthalpic contacts between monomers and solvent. At the $\Theta$-temperature $T_\Theta$ ($\chi = 0.5$), the entropic and enthalpic forces are balanced, leading to an ideal Gaussian chain conformation with $\nu = 1/2$.

Polymer conformation and architecture cause changes in $T_\Theta$ due to changes in configurational entropy and local monomer density. Previous experimental investigations and simulations revealed a suppression of $T_\Theta$ for rings[6–9] and branched chains[10–15] in comparison to linear chains. By contrast, polymer-grafted nanoparticles are a separate class of material with a finite-sized core of different chemistry and high grafting density with often hundreds of grafted chains per particle. Many parameters, such as the core size, grafting density, grafted molecular weight, and interactions between the grafted chains and the core, may affect the interaction between the grafted chains and their surrounding environment to guide and control the conformation of the grafted polymer[16] and the morphology and dispersion state of the grafted particles by tuning the competition between enthalpic and entropic forces.[17,18] Whereas this competition is well understood for free chains, how topologically constraining the chains to a hard surface *via* grafting affects these forces

[a] *Materials Science and Engineering, University of Houston, Houston, TX 77204, USA*
[b] *Department of Chemical and Biomolecular Engineering, University of Houston, Houston, TX 77204, USA. E-mail: ramanan@uh.edu*
[c] *National Institute of Standards and Technology Center for Neutron Research, Gaithersburg, MD 20899, USA*
[d] *Department of Materials Science and Engineering, University of Maryland, College Park, MD 20742, USA*

† Electronic supplementary information (ESI) available. See DOI: 10.1039/c8sm00929e

‡ Authors contributed equally to this work.

§ Present address: Department of Physics, Virginia Tech, Blacksburg, VA 24061, USA.

remains an open question. Understanding these fundamental interactions between polymer-grafted nanoparticles and the surrounding solvent is important to design processing conditions for nanocomposite materials and targeted drug-delivery applications.

Here, we find that the $\Theta$-temperature of grafted polymer chains is suppressed relative to that of free chains in dilute solutions. Using small angle neutron scattering (SANS), we measure the conformation of polystyrene chains grafted to silica nanoparticles dispersed in deuterated cyclohexane. The solvent quality of cyclohexane for polystyrene changes as a function of temperature, allowing for structural measurements of the grafted chains with varying solvent quality. At high temperatures, cyclohexane acts as a good solvent for the polystyrene chains, swelling the grafted corona and stretching the chains. At lower temperatures, the grafted corona initially compresses as solvent is expelled before precipitously shrinking below $T_\Theta$, leading to aggregation and sedimentation.[19] We find $T_\Theta \approx 34$ °C for the polymer-grafted nanoparticles (PGNPs) dispersed in $d_{12}$-cyclohexane, which is significantly suppressed from $T_\Theta = 38$ °C for free polystyrene chains in the same solvent.[20–23] These conformational changes and suppression of $T_\Theta$ arise from the balance between enthalpic and entropic forces acting on the grafted polymer chains.

## 2 Results and discussion

As an initial characterization, the hydrodynamic radius $R_H$ of polystyrene-grafted nanoparticles dispersed in protonated cyclohexane was calculated from dynamic light scattering measurements (Fig. 1).¶ Protonated cyclohexane and polystyrene is a well-studied system that allows us to determine how polymer-grafted nanoparticles respond to changes in solvent quality. To highlight the change in particle radius with changing temperatures, we normalize measurements to the radius at 50 °C. At high temperatures, cyclohexane is a good solvent for polystyrene and the grafted nanoparticles are well dispersed. Initially, the radius decreases with decreasing temperature by ~10%. This change in hydrodynamic size suggests a shrinking grafted corona and is qualitatively consistent with a decrease in solvent quality as the temperature approaches the theta temperature $T_\Theta = 34.5$ °C for free polystyrene chains in protonated cyclohexane.[24] Here, it is important to note that $T_\Theta$ depends significantly on the isotopical composition of the solvent, increasing from 34.5 °C for *protonated* cyclohexane to 38 °C for deuterated cyclohexane.[20–23] For $T < 34.5$ °C, protonated cyclohexane becomes a poor solvent for polystyrene, and the grafted particles ultimately become unstable and aggregate, resulting in a sharp increase in $R_H$. This complex thermal dependence of $R_H$ derives from the molecular interactions between polystyrene and cyclohexane. The DLS measurements do not directly probe the structure of the polymer or the nature of the polymer–solvent interactions but rather allow for interpretation of effective hydrodynamic changes and macroscale phenomena such as aggregation and phase separation.

¶ Error bars represent one standard deviation in this plot and throughout the manuscript.

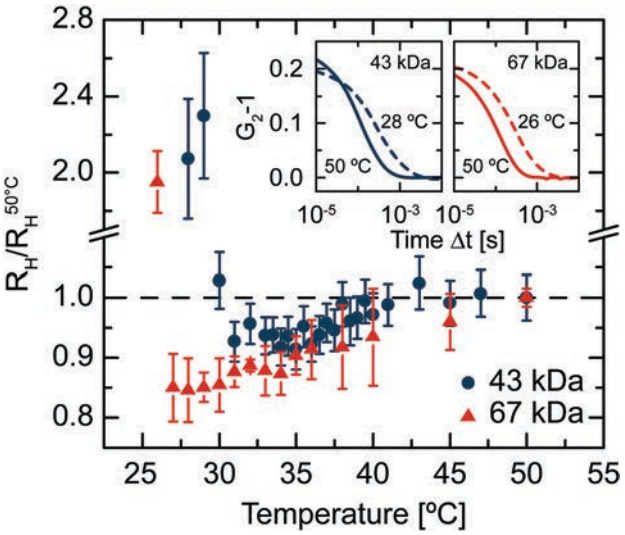


Fig. 1 Normalized hydrodynamic radius $R_H/R_H^{50°C}$ of nanoparticles grafted with (blue) 43 kDa and (red) 67 kDa polystyrene dispersed in cyclohexane as a function of temperature (±0.5 °C). Insets: Intensity correlation function $G_2 - 1$ as a function of time $\Delta t$ for grafted nanoparticles at high (solid) and low (dashed) temperatures. Estimated accuracy on temperature is ±0.5 °C.

To directly measure the conformational changes of the grafted chains and the nature of polymer–solvent interactions, we use small-angle neutron scattering. For SANS measurements, the grafted particles are dispersed in fully deuterated cyclohexane to decrease incoherent scattering $I_{incoh}$ and increase the scattering contrast of the polymer. Corresponding to different structures, the coherent intensity $I_{coh}$ at high and low $Q$ exhibit a striking difference in their thermal response (Fig. 2). For $Q = 0.15$ Å$^{-1}$, $I_{coh}$ is dominated by intra- and interchain scattering of the polymer chains within the grafted corona and decreases monotonically with decreasing temperature for both molecular weights. By contrast, $I_{coh}$ at $Q = 0.004$ Å$^{-1}$ is clearly non-monotonic, exhibiting a maximum at $T \approx 35$ °C. At this wavevector, $I_{coh}$ is dominated by the spherical morphology of the polymer-grafted nanoparticle and initially increases with decreasing temperature before decreasing by over an order of magnitude for $T < 35$ °C. Along with the long equilibration times (≈30 min) used in these experiments, the reproducibility of these trends between particles grafted with different molecular weights indicate that the polymer conformations are equilibrium structures.

The qualitative difference in the temperature dependence of the scattering intensity in different wavevector ranges originates from changes in the structure of the polymer-grafted nanoparticles at different length scales. There has been substantial interest in modeling the conformations of polymers grafted to a spherical core, with success in assuming a corona of non-interacting Gaussian[25,26] or extended[27] chains or as sphere with gradations in scattering length density.[28] In this system, however, the significant polymer–solvent interactions affect the

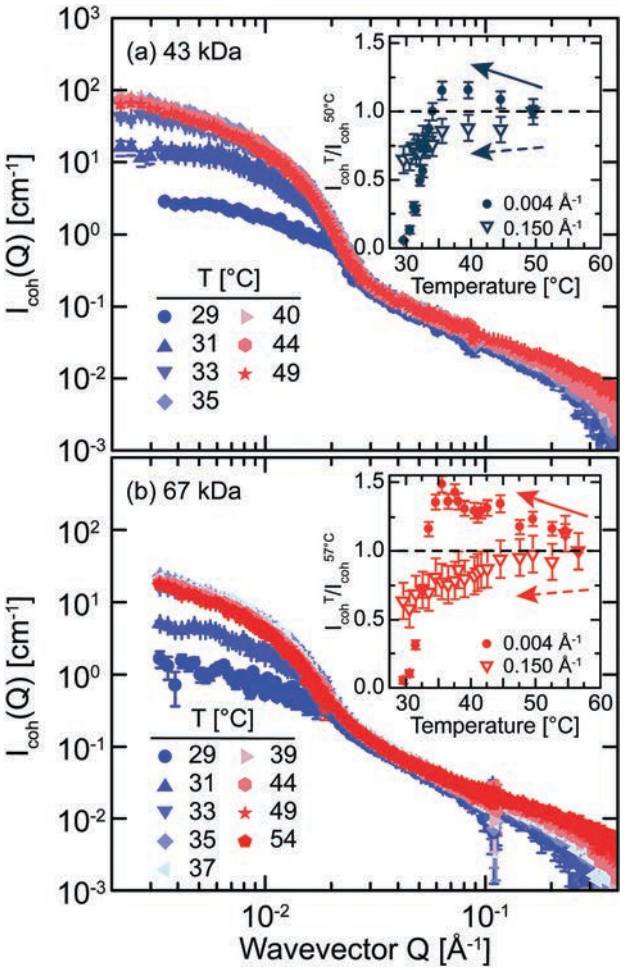


Fig. 2 Coherent scattering intensity $I_{coh}(Q)$ as a function of wavevector $Q$ for polystrene-grafted nanoparticles with molecular weights $M_w$ of (a) 43 kDa and (b) 67 kDa dispersed in $d_{12}$-cyclohexane at various temperatures. Insets: $I_{coh}$ as a function of temperature normalized by the scattering intensity at high temperature for wavevectors $Q$ = 0.004 and 0.15 Å$^{-1}$.

grafted polymer conformations and the measured scattering intensity. Additionally, and perhaps because of the low scattering intensity, we do not observe oscillations or changes in slope of the high-$Q$ portion of the scattering curve that are often characteristic of form factors for multi-shell particles or particles with complex SLD profiles. Within the resolution of the data, fits with complex SLD profiles are indistinguishable from those of the core–shell model or do not capture the scattering intensity across the full wavevector range (ESI†). Thus, recognizing that the grafted corona resembles a semidilute polymer solution on shorter length scales and that on a larger scale the polymer-grafted nanoparticle resembles a spherical core with a polymer coating, we fit the total scattering intensity $I_{tot}$ to the sum of Lorentzian $P_{Lorentz}$ and core–shell[29] $P_{CS}$ form factors with an incoherent contribution $I_{incoh}$ (eqn (1)–(3)).

$$I_{tot}(Q) = P_{Lorentz}(Q) + P_{CS}(Q) + I_{incoh} \quad (1)$$

$$P_{Lorentz}(Q) = \frac{A}{1 + (Q\xi)^{1/\nu}} \quad (2)$$

$$P_{CS}(Q) = \frac{\phi}{V}\left[3V_c(\rho_c - \rho_s)\frac{\sin(QR_c) - QR_c\cos(QR_c)}{(QR_c)^3} + 3V_s(\rho_s - \rho_{solv})\frac{\sin(QR) - QR\cos(QR)}{(QR)^3}\right]^2 \quad (3)$$

With a large number of fitting parameters, this model requires careful implementation. The following parameters are known *a priori* for each suspension and are held fixed at all temperatures: the SLDs of the silica core $\rho_c$ and solvent $\rho_{solv}$, the total volume fraction $\phi$ of polymer-grafted nanoparticles, and the radius $R_c$ = 6.0 nm of the silica core.[30] The Lorentzian form factor excellently fits the scattering intensity of semidilute solutions of free polymer chains in the presence of nanoparticles[31] where $\xi$ is the correlation length between polymer chains. For semidilute solutions, the polymer density is constant throughout the solution on length scales longer than $\xi$. By contrast, the density profile of grafted chains on spherical particles decreases with radial distance so that the polymer concentration is highest at the particle surface and geometrically controlled by the polymer grafting density $\sigma$ according to $\xi = \sqrt{4/\pi\sigma}$.[32] This reduces the fit variables to the following parameters: the excluded volume parameter $\nu$ of the grafted chains, the SLD of the grafted corona $\rho_s$, and the thickness $H$ grafted corona. We also note that, for simplicity, this model neglects cross scattering between the grafted chains and the silica core which is expected to be negligible in this case. The arbitrary Lorentzian scaling $A$ and incoherent contributions $I_{incoh}$ are fit globally over all temperatures for both the 43 kDa and 67 kDa samples. The contributions from the core and shell are scaled by the volumes of each where $V$ is the specific volume of a polymer-grafted nanoparticle with radius $R = H + R_c$, $V_c$ is the specific volume of the core with radius $R_c$, and the $V_s = V - V_c$ is the specific volume of the shell. Additionally, the core and shell are both polydisperse, so eqn (3) is numerically integrated over two log-normal distributions with log-normal dispersities of $\sigma_c$ = 0.28 for the core and a floating $\sigma_s$ for the shell during the fitting algorithm. Using this methodology, the fits agree well with the measured data across both grafted molecular weights, all wavevectors, and all temperatures (Fig. 3).

The fitted parameters from the modeling of the SANS data provide quantitative measurements on the structure of the polymer-grafted nanoparticles and on the conformational response to temperature changes. At high temperatures $T > 34$ °C where cyclohexane acts as a good solvent ($\chi < 0.5$), the grafted corona is extended with a nearly constant thickness with the higher molecular weight brushes forming a thicker grafted layer (Fig. 4(a)), in qualitative agreement with theoretical models[33–35] that give $H \sim M_w^{3/5}$. Similarly extended coronas have been observed for dispersions of grafted nanoparticles in good solvent.[16] As the temperature decreases below $T < 34$ °C, the grafted layers collapse dramatically by approximately 50%, indicating that the monomer–solvent interaction becomes less favorable than the monomer–monomer interaction (*i.e.* $\chi > 0.5$). This collapse contains data from two heating–cooling cycles, indicating that the structural changes are reversible. The observed

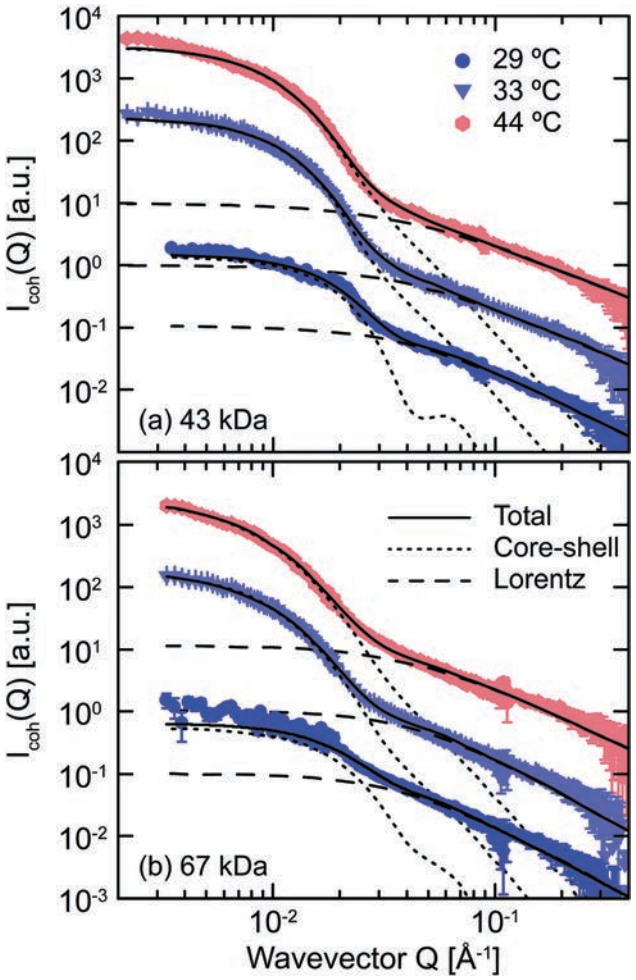


Fig. 3 Coherent scattering intensity $I_{coh}(Q)$ for (a) 43 kDa and (b) 67 kDa polymer-grafted nanoparticles in $d_{12}$-cyclohexane at various temperatures. Solid curves are best fits to the sum of core–shell (dotted) and Lorentzian (dashed) form factors. Data and curves shifted vertically for clarity.

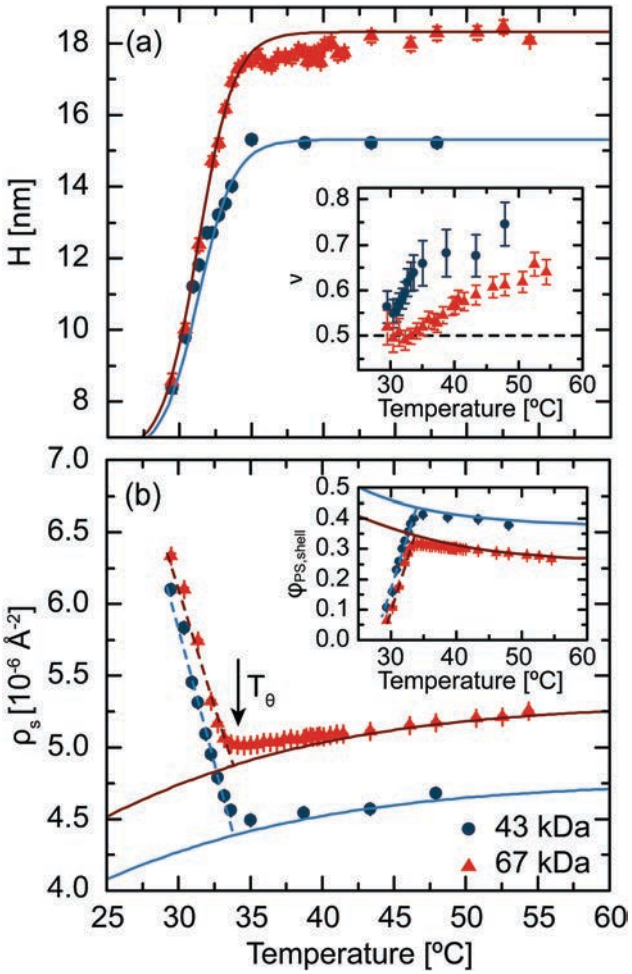


Fig. 4 (a) Thickness $H$ of the grafted layer as a function of temperature for grafted molecular weights of 43 (blue) and 67 kDa (red). Inset: Excluded volume parameter $\nu$ for the grafted polymer as a function of temperature. Dashed line indicates $\nu = 0.5$ prediction for Gaussian chains in a $\Theta$-solvent. (b) Scattering length density of the grafted layer $\rho_s$ as a function of temperature. Inset: Effective volume fraction of polystyrene in the grafted layer $\varphi_{PS,shell}$ calculated from eqn (4) as a function of temperature. All curves are guides to the eye. Estimated accuracy on temperature is ±0.5 °C.

changes in the dispersion and corona thickness, which are comparable to those identified by DLS (Fig. 1) are expected to emerge from changes in the conformational state of the grafted polymer chains.

The conformation of individual grafted chains is captured by the excluded volume parameter $\nu$ (inset to Fig. 4(a)). Consistent with the swollen morphology of the corona at high temperatures, the individual polymer chains are more extended than free chains in a good solvent ($\nu > 0.588$). It is well known that grafted polymers are stretched normal to the grafted surface to balance the overlap between neighboring chains and the loss of configurational entropy from stretching.[36,37] Because the monomer density decreases radially from the particle surface for grafted chains, the degree of stretching will also decrease with radial distance. The present SANS model, however, averages the stretching exponent over all radial distances so that the average stretching exponent in the thicker 67 kDa shell is lower than that of the thinner 43 kDa shell. As the temperature and solvent quality decreases, $\nu$ decreases monotonically to approach $\nu = 1/2$ for both molecular weights, rather than the globule conformation with $\nu = 1/3$ observed for dilute solutions of free chains. The difference arises from the local polymer concentration. Although the concentration of PGNPs is dilute, the end-tethering of the grafted polymer forces the local polymer concentration near the particle to be high. Whereas dilute free chains in solution can only expel solvent by collapsing onto themselves and forming intramolecular contacts, the grafted polymer forms both intra- and intermolecular contacts with neighboring chains to expel solvent. Thus, the grafted polymer chains adopt melt-like Gaussian conformations around the particle surface in which the excluded volume effects are fully screened (*i.e.* $\nu = 1/2$). We expect the transition between globule and melt-like Gaussian conformations to be dependent on the polymer grafting density. When the grafting density is low *i.e.* $\sigma < 1/R_g^2$, the grafted chains will be isolated, unable to form intermolecular contacts, and should collapse into globules.

The expulsion of solvent from the grafted layer is captured by the SLD of the shell $\rho_s$ (Fig. 4(b)), which is bounded by $\rho_{PS}$ and $\rho_{solv}$ according to the mixing rule

$$\rho_s = \varphi_{PS,shell}\rho_{PS} + (1 - \varphi_{PS,shell})\rho_{solv}, \quad (4)$$

where $\varphi_{PS,shell}$ is the volume fraction of polystyrene in the grafted corona. The 43 kDa sample has a lower $\rho_s$ and a higher concentration of polystyrene in the shell (inset to Fig. 4(b)) compared to that of the 67 kDa sample. The higher concentration of polymer in the shell more strongly stretches the 43 kDa chains, consistent with the larger excluded volume parameter $\nu$ (inset to Fig. 4(a)). As a function of temperature, the measured $\rho_s$ exhibits the same non-monotonic trend as $I_{coh}(Q)$ for $Q = 0.004$ Å$^{-1}$ (insets for Fig. 2). As $T$ decreases towards 34 °C, the fraction of polymer in the shell increases as solvent is expelled due to the decreasing solvent quality of cyclohexane. For $T < 35$ °C, however, $\rho_s$ increases dramatically. This non-monotonic trend is due to the convolution of two fitting parameters, $\phi$ and $\rho_s$. With our fitting form, these two parameters are directly correlated and difficult to separate. We *a priori* defined $\phi$ according to sample preparation and left $\rho_s$ to float. While this is a good assumption when the PGNPs are well dispersed, once cyclohexane becomes a poor solvent, the PGNPs aggregate and crash out of solution, resulting in an effectively less-concentrated dispersion within the neutron beam. This decrease in $\phi$ deviates from the constant-$\phi$ assumption, leading to a decrease in $I_{coh}(Q)$ at low $Q$ and an artificial increase in the fitted value of $\rho_s$. Recognizing that the aggregation of PGNPs is analogous to the cloud-point in a polymer solution, we use the inflection point of $\rho_s$ to quantify $T_\Theta$.

For dilute polymer solutions, $T_\Theta$ is defined as the temperature at which the enthalpic and entropic forces are balanced and lead to an ideal Gaussian conformation ($\chi = 0.5$). Crossing $T_\Theta$ induces a coil-to-globule transition for free chains.[5] For PGNPs, however, there are multiple physical changes that must happen – an initial polymer collapse followed by subsequent particle aggregation and finally sedimentation through the solvent. Such a multi-step mechanism is reminiscent of the morphological change for PGNPs dispersed in chemically distinct polymer matrices.[30,38] Fundamentally, the driving physics is analogous for PGNPs dispersed in a chemically distinct melt and in a solvent. Once the solvent – whether a small molecule or a large macromolecule – has an unfavorable interaction with the grafted chains, the grafted polymers collapse to expel the solvent. The dewetting transition generates an unfavorable interface between the grafted polymers and the solvent and forces the PGNPs to aggregate to reduce the interfacial area.[39] These are distinct transitions and occur at well-separated temperatures in a melt.[30] In a solvent system as studied here, the different physical changes appear to occur at nearly the same temperature. Indeed, the inflection point in $\rho_s$ (Fig. 4(b)) corresponds closely to the temperature at which $\nu = 0.5$ for the 67 kDa sample and at which the grafted layer thickness decreases rapidly (Fig. 4(a)). For this system specifically of polystyrene grafted nanoparticles dispersed in $d_{12}$-cyclohexane, $T_\Theta \approx 34$ °C (Fig. 4), which is significantly suppressed relative to $T_\Theta = 38$ °C for free polystyrene chains dissolved in $d_{12}$-cyclohexane.[20–23]

Similar $T_\Theta$ suppression has been observed for polymers with complex architectures, *e.g.* cyclic rings, stars, and combs. Whereas complex polymer architectures can be approximated as individual chains branching from atomic-sized junction points, PGNPs are composed of individual chains tethered to a finite-sized core. Surprisingly, tethered chains and polymers with complex architectures have similar $T_\Theta$; the magnitude of suppression in $T_\Theta$ from that of linear chains observed here for PGNPs is comparable to the suppression for polymers with other complex architectures. Because $T_\Theta$ represents the temperature at which entropic and enthalpic forces are balanced, the suppression of $T_\Theta$ for PGNPs must result from changes in the entropy and enthalpy of mixing. Due to the loss of translational freedom, the change in the entropy of mixing $\Delta S_{mix}$ from a swollen to collapsed state is lower for a grafted chain than for a free chain,[40] which drives $T_\Theta$ higher. On the other hand, the enthalpy of mixing $\Delta H_{mix}$ for a grafted chain is lower than that of a free chain because the high local polymer concentration near the particle surface screens some of the contacts between grafted chains and solvent molecules. The tethering to the particle surface restricts the grafted chains close to each other in contrast to free chains which diffuse away from each other to maximize solvent–monomer contacts. The resulting decrease in $\Delta H_{mix}$ drives $T_\Theta$ lower. Thus, the structure of PGNPs results from competing enthalpic and entropic forces, which are difficult to predict or measure independently. Based on the experiments reported here, the enthalpic forces must dominate to suppress $T_\Theta$. A critical test of this theory would be to measure the conformational changes of isolated grafted chains for which $\Delta S_{mix}$ will be reduced by end-tethering but for which $\Delta H_{mix}$ will be unaffected by changes in local polymer density.

# 3 Conclusion

We probe the conformational changes of polystyrene chains grafted to silica nanoparticles dispersed in $d_{12}$-cyclohexane as a function of temperature using SANS. At high temperatures, the grafted nanoparticles are well-dispersed in the solvent with a swollen corona. At low temperatures, the grafted chains collapse and expel the solvent, destabilizing the particle suspension and leading to aggregation. From the structural measurements, we determine the $\Theta$-temperature of the polymer-grafted nanoparticles to be $\approx$34 °C, suppressed from 38 °C for free chains. The change in $\Theta$-temperature arises from competing entropic and enthalpic forces, with the enthalpic interactions dominating for this system. Because the structure and interactions of polymer-grafted nanoparticles strongly depend on many parameters such as the particle size, grafted molecular weight, and grafting density, future work should aim to understand how these parameters control the balance between enthalpic and entropic interactions. The dominance of enthalpic contributions elucidated by this work underlines the importance of understanding the fundamental physics controlling the structure and

 

phase transitions of polymer-grafted nanoparticles, with implications on how solution processing can affect the structure of polymer nanocomposite materials.

# 4 Materials and methods

## 4.1 Synthesis of initiator-grafted $SiO_2$ nanoparticles

The 1-(chlorodimethylsilyl)propyl 2-bromoisobutyrate initiator was synthesized using a previously described procedure.[41] The initiator was then added to a dispersion of $SiO_2$ nanoparticles (≈30% by weight in methyl isobutyl ketone, average radius $R$ = 6 nm with a log-normal polydispersity of 0.28, Nissan Chemical America‖) and reacted under gentle reflux at 85 °C overnight.[42] Hexamethyldisilazane (Sigma-Aldrich, 99.9%) was added to the dispersion and reacted to cap any remaining unfunctionalized hydroxyl groups on the silica surface and subsequently washed and dried as described previously.[30]

## 4.2 Synthesis of polystyrene-grafted $SiO_2$ nanoparticles

Polystyrene was synthesized from the surface of the initiator-functionalized nanoparticles using a modified AGET ATRP procedure.[43] The particles were washed multiple times by redissolving in tetrahydrofuran and precipitating in cold methanol before drying under vacuum. The grafted polymers were characterized after being cleaved from the $SiO_2$ surface by dissolving the grafted nanoparticles in THF, adding 2% solution of aqueous hydrofluoric acid, and reacting overnight. The synthesized polystyrene had weight-averaged molecular weights $M_W$ = 43 and 67 kDa with dispersities $Đ \equiv M_W/M_N$ = 1.2 and 1.3, respectively. Grafting densities were determined to be $\sigma$ = 0.16 and 0.26 chains per nm$^2$, respectively, using thermal gravimetric analysis.

## 4.3 Dynamic light scattering

Polystyrene-grafted $SiO_2$ nanoparticles were dissolved in cyclohexane at a concentration of 0.3 mg mL$^{-1}$ (volume fraction $\phi \approx 2.5 \times 10^{-4}$) at 50 °C for 24 h, sonicated for 10 min, and filtered through a 0.2 μm PTFE filter. Dynamic light scattering (DLS) data were collected on a Brookhaven Instruments goniometer (BI-200SM, Brookhaven Instruments Corporation) at scattering angles of 60°, 90°, and 120° with an incident wavelength $\lambda$ = 637.6 nm (Mini-L30 laser source). Samples were allowed to equilibrate at each temperature for 30 minutes before collection. The measured intensity correlation functions $G_2(Q,\Delta t)$ were fit using the Siegert relation and cumulant expansion[44] $G_2(Q,\Delta t) = A + BG_1^2(Q,\Delta t)$, where $A \approx 1$ relates to the autocorrelation at long times, $B \approx 1$ represents the autocorrelation of the particles at short times, and $G_1(Q,\Delta t) = \exp(-\Gamma\Delta t)(1 + \mu\Delta t^2/2)$ is the intermediate scattering function with an average relaxation rate $\Gamma$ and a polydispersity of $\mu/\Gamma^2$. The diffusivity $D$ of the polymer-grafted nanoparticles is calculated by fitting $\Gamma = DQ^2$. Finally, the hydrodynamic radius $R_H$ is determined using the Stokes–Einstein equation $R_H = k_BT/(6\pi\eta D)$, where $k_B$ is the Boltzmann constant and $\eta$ is the temperature-dependent solvent viscosity.

‖ The identification of any commercial product or trade name does not imply endorsement or recommendation by the National Institute of Standards and Technology.

## 4.4 Small-angle neutron scattering

Polystyrene-grafted nanoparticles were dissolved in fully deuterated $d_{12}$-cyclohexane at concentrations of 3.4 mg mL$^{-1}$ ($\phi \approx 2.9 \times 10^{-3}$) and 1.7 mg mL$^{-1}$ ($\phi \approx 1.5 \times 10^{-3}$) for the 43 kDa and 67 kDa samples, respectively. Samples were stirred at 50 °C for at least 24 hours to ensure complete dissolution and then loaded into quartz banjo sample cells. The neutron scattering length densities (SLDs) of polystyrene $\rho_{PS}$, silica $\rho_{SiO_2}$, and $d_{12}$-cyclohexane $\rho_{solv}$ are 1.41, 3.48, and 6.67 × 10$^{-6}$ Å$^{-2}$, respectively. Small angle neutron scattering (SANS) measurements were collected over a wavevector range 0.002 Å$^{-1}$ < $Q$ < 0.5 Å$^{-1}$ at the NGB30 beamline at the Center for Neutron Research, National Institute of Standards and Technology. Samples were placed in a holder with a temperature-controlled fluid circulation system and allowed to equilibrate at each temperature for 30 minutes before data collection. The raw SANS data is corrected for detector sensitivity, empty cell scattering, and blocked beam scattering and is normalized to absolute intensity $I(Q)$ using IgorPro.[45]

# Conflicts of interest

There are no conflicts to declare.

# Acknowledgements

We thank Jialin Qiu for helpful discussions and Dr. Jeffrey Rimer for access to the dynamic light scattering instrument. This work utilized the NIST Center for Neutron Research (NCNR) supported in part by the National Science Foundation (NSF) under Agreement No. DMR-1508249.

# References

1 M. L. Huggins, *J. Chem. Phys.*, 1941, **9**, 440.
2 P. J. Flory, *J. Chem. Phys.*, 1942, **10**, 51–61.
3 P. J. Flory and W. R. Krigbaum, *J. Chem. Phys.*, 1950, **18**, 1086–1094.
4 P. J. Flory and W. R. Krigbaum, *Annu. Rev. Phys. Chem.*, 1951, **2**, 383–402.
5 G. Swislow, S. T. Sun, I. Nishio and T. Tanaka, *Phys. Rev. Lett.*, 1980, **44**, 796–798.
6 J. Roovers and P. M. Toporowski, *Macromolecules*, 1983, **16**, 843–849.
7 J. Roovers, *J. Polym. Sci., Polym. Phys. Ed.*, 1985, **23**, 1117–1126.
8 J. Suzuki, A. Takano and Y. Matsushita, *J. Chem. Phys.*, 2011, **135**, 204903.
9 A. Narros, A. J. Moreno and C. N. Likos, *Macromolecules*, 2013, **46**, 3654–3668.
10 T. A. Orofino and F. Wenger, *J. Phys. Chem.*, 1963, **67**, 566–575.

11 J.-G. Zilliox, *Die Makromol. Chemie*, 1972, **156**, 121–141.
12 F. Candau, C. Strazielle and H. Benoit, *Die Makromol. Chemie*, 1973, **170**, 165–176.
13 J. Roovers, *Polymer*, 1979, **20**, 843–849.
14 C. Tsitsilianis, E. Pierri and A. Dondos, *J. Polym. Sci., Polym. Lett. Ed.*, 1983, **21**, 685–691.
15 N. Khasat, R. W. Pennisi, N. Hadjichristidis and L. J. Fetters, *Macromolecules*, 1988, **21**, 1100–1106.
16 A. T. Lorenzo, R. Ponnapati, T. Chatterjee and R. Krishnamoorti, *Faraday Discuss.*, 2016, **186**, 311–324.
17 S. K. Kumar, N. Jouault, B. Benicewicz and T. Neely, *Macromolecules*, 2013, **46**, 3199–3214.
18 K. J. Modica, T. B. Martin and A. Jayaraman, *Macromolecules*, 2017, **50**, 4854–4866.
19 A. Kaiser and A. M. Schmidt, *J. Phys. Chem. B*, 2008, **112**, 1894–1898.
20 C. Strazielle and H. Benoit, *Macromolecules*, 1975, **8**, 203–205.
21 B. Farnoux, F. Boue, J. Cotton, M. Daoud, G. Jannink, M. Nierlich and P. De Gennes, *J. Phys.*, 1978, **39**, 77–86.
22 Y. Melnichenko, M. Anisimov, A. Povodyrev, G. Wignall, J. Sengers and W. Van Hook, *Phys. Rev. Lett.*, 1997, **79**, 5266–5269.
23 A. Siporska, J. Szydlowski and L. P. N. Rebelo, *Phys. Chem. Chem. Phys.*, 2003, **5**, 2996–3002.
24 H. Elias, in *Polymer Handbook*, ed. J. Brandup, E. Immergut and E. Grulke, John Wiley, New York, 4th edn, 1999, pp. VII 291–VII 326.
25 J. S. Pedersen and M. C. Gerstenberg, *Macromolecules*, 1996, **29**, 1363–1365.
26 J. S. Pedersen and M. C. Gerstenberg, *Colloids Surf., A*, 2003, **213**, 175–187.
27 M. J. A. Hore, J. Ford, K. Ohno, R. J. Composto and B. Hammouda, *Macromolecules*, 2013, **46**, 9341–9348.
28 T. Foster, *J. Phys. Chem. B*, 2011, **115**, 10207–10217.
29 A. Guinier and G. Fournet, *Small-Angle Scattering of X-Rays*, John Wiley and Sons, New York, 1955.
30 T. B. Martin, K. I. S. Mongcopa, R. Ashkar, P. Butler, R. Krishnamoorti and A. Jayaraman, *J. Am. Chem. Soc.*, 2015, **137**, 10624–10631.
31 R. Poling-Skutvik, K. I. S. Mongcopa, A. Faraone, S. Narayanan, J. C. Conrad and R. Krishnamoorti, *Macromolecules*, 2016, **49**, 6568–6577.
32 R. Poling-Skutvik, K. N. Olafson, S. Narayanan, L. Stingaciu, A. Faraone, J. C. Conrad and R. Krishnamoorti, *Macromolecules*, 2017, **50**, 7372–7379.
33 M. Daoud and J. Cotton, *J. Phys.*, 1982, **43**, 531–538.
34 E. B. Zhulina, O. V. Borisov, V. A. Pryamitsyn and T. M. Birshtein, *Macromolecules*, 1991, **24**, 140–149.
35 D. Dukes, Y. Li, S. Lewis, B. Benicewicz, L. Schadler and S. K. Kumar, *Macromolecules*, 2010, **43**, 1564–1570.
36 S. Milner, T. Witten and M. Cates, *Macromolecules*, 1988, **21**, 2610–2619.
37 S. T. Milner, *Science*, 1991, **251**, 905–914.
38 T. B. Martin and A. Jayaraman, *Macromolecules*, 2016, **49**, 9684–9692.
39 R. Zhang, B. Lee, M. R. Bockstaller, S. K. Kumar, C. M. Stafford, J. F. Douglas, D. Raghavan and A. Karim, *Macromolecules*, 2016, **49**, 3965–3974.
40 P. G. de Gennes, *Macromolecules*, 1980, **13**, 1069–1075.
41 R. Ponnapati, O. Karazincir, E. Dao, R. Ng, K. K. Mohanty and R. Krishnamoorti, *Ind. Eng. Chem. Res.*, 2011, **50**, 13030–13036.
42 J. Pyun, S. Jia, T. Kowalewski, G. D. Patterson and K. Matyjaszewski, *Macromolecules*, 2003, **36**, 5094–5104.
43 W. Jakubowski and K. Matyjaszewski, *Macromolecules*, 2005, **38**, 4139–4146.
44 B. J. Frisken, *Appl. Opt.*, 2001, **40**, 4087–4091.
45 S. R. Kline, *J. Appl. Crystallogr.*, 2006, **39**, 895–900.

 